Expert Systems With Applications 226 (2023) 120244

Contents lists available at ScienceDirect

Expert Systems With Applications

journal homepage: www.elsevier.com/locate/eswa

Intelligent fault diagnosis for triboelectric nanogenerators via a novel deep learning framework

Hao Wu [a], Xing'ang Xu [b,*], Chuanfu Xin [a], Yichen Liu [a], Runze Rao [a], Zhongjie Li [a,c,d], Dan Zhang [a,d], Yongxi Wu [e], Senzhe Han [f]

[a] School of Mechatronic Engineering and Automation, Shanghai University, Shanghai 200444, PR China
[b] School of Naval Architecture and Ocean Engineering, Dalian University of Technology, Dalian 116024, PR China
[c] School of Artificial Intelligence, Shanghai University, Shanghai 200444, PR China
[d] Engineering Research Center of Unmanned Intelligent Marine Equipment, Shanghai University, Shanghai 200444, PR China
[e] School of Mechanics and Engineering Science, Shanghai University, Shanghai 200444, PR China
[f] Shanghai Electric Wind Power Group Co., Ltd., Shanghai 200235, PR China

ARTICLE INFO

Keywords:
Triboelectric nanogenerator
Intelligent fault diagnosis
Deep learning
Real-time

ABSTRACT

Triboelectric nanogenerators (TENGs) provide a new approach to converting mechanical energy into electric power. Although many researchers have made progress in the improvement of the electric output of TENG, the service life of the electronic components in TENG is generally shorter than that of the stator or rotor windings in conventional generators. Considering that the fault of electronic components in TENG results in a decline in the electric output, which may subsequently increase the usage cost and even endanger the users of the TENG-based self-power devices. Thus, it is necessary to provide parametric schemes for the high-reliable iterative optimization design of TENG by identifying the fault-susceptible components in TENG. This study proposes a novel deep learning framework based on an attention neural network (AttCNN) for the fault diagnosis of TENG. The proposed method integrates the attention mechanism and convolutional network. Therein, the global correlation features in voltage signals extracted by the attention mechanism can effectively reflect the status variation of TENG among different moments, and the feature information extracted by the convolutional network guarantees the fault diagnosis efficiency of TENG. Thereby the proposed method fills in the gaps in the field of fault diagnosis for TENG. In the case study, the fault diagnosis performance of the proposed method for an experimental TENG is analyzed. The results indicate that the predicted and real status of TENG are in good agreement, validating the effectiveness of the proposed method for the fault diagnosis of TENG. Moreover, the results reveal that the proposed method possesses a promising generalization performance, demonstrating the feasibility of the application of the proposed method for the real-time fault diagnosis of TENG. A comparative analysis illustrates that the performance of the proposed method is better than that of recently published data-driven methods in terms of fault diagnosis accuracy and efficiency. Hence, the results of the case study indicate that the proposed method has the characteristic of high efficiency, high accuracy, and well-generalization, thereby the application of the proposed method is conducive to the safe operation of TENG.

1. Introduction

Numerous power energy is required with the rapid development of the global economy (Qadir et al., 2021). Nowadays, coal, oil, and other non-renewable resources are severely consumed (Islam, Mekhilef, & Saidur, 2013), meanwhile, energy dissipation and unreasonable utilization of energy are also common due to mechanical vibration or other unavoidable phenomena (Hidalgo-Leon et al., 2022; Qi et al., 2022; Zhu, Yang, et al., 2023). Therefore, the development of clean and efficient energy or improving energy utilization has become a hot issue (Wang, Jiang, et al., 2022; Wang, Gao, et al., 2022; Zhu, Wen, et al., 2023).

Aiming to collect and utilize friction-loss energy, a triboelectric nanogenerator (TENG) was developed in 2012 (Fan, Tian, & Lin Wang, 2012). As an emerging kind of generator, TENG can convert the mechanical energy in the environment into electric energy through the effect of triboelectrification and electrostatic induction (Zhu et al.,

* Corresponding author.
E-mail address: xuxingang@mail.dlut.edu.cn (X. Xu).

https://doi.org/10.1016/j.eswa.2023.120244
Received 17 November 2022; Received in revised form 23 March 2023; Accepted 22 April 2023
Available online 28 April 2023

2022). Moreover, TENG has the characteristics of a simple structure, low cost, high integration, and many kinds of prepared materials (Xin et al., 2022; Zhu et al., 2021). Hence, TENG has been widely applied in environmental mechanical energy harvesting and self-powered sensors (Li et al., 2022; Xu, Li, et al., 2022; Zhao, Fan, et al., 2022; Zhu et al., 2020).

The output performance of TENG is significantly affected by the electronic components (electrode, triboelectric layer, and interlayer embedding between the triboelectric layer and electrode). However, compared with the stator or rotor windings in conventional generators, the service life of the electronic components of TENG, especially triboelectric layers or interlayers, is limited (Cheng, Gao, & Wang, 2019). Moreover, the relative motion of the positive/negative triboelectric layers directly affects the electric output of TENG, while the process of the relative motion is susceptible to interference from the external environment (Cheng et al., 2019). Thus, although TENG provides a new approach for converting mechanical energy into electric power, the fault susceptibility of TENG may increase additional costs and even endanger the users of the TENG-based self-power devices. Thereby it is necessary to provide parametric schemes for the high-reliable iterative optimization design of TENG by identifying the fault-susceptible components in TENG. As referred from Ref. (Lei et al., 2020), a timely fault diagnosis can effectively identify the fault location and suppress the further deterioration of the fault in generators. So, an efficient and accurate fault diagnosis for TENG is in demand.

However, the existing studies mainly focused on the enhancement of the output performance or industrial application of TENG (Lone et al., 2022). For instance, to enhance the electric output of TENG, Kim et al. (Kim et al., 2019) and Huang et al. (Huang et al., 2019) developed enhanced TENGs through the approaches of surface modification and microstructure, respectively, moreover, Feng et al. (Feng et al., 2017) and Xin et al. (Xin et al., 2022) embedded interlayers between the triboelectric layer and electrode, thereby reducing charge diffusion by store charges or block charges to (Chun et al., 2016). In terms of the industrial application of TENG, Xiang et al. (Xiang, Yang, Cao, & Wang, 2022) and Yuan et al. (Yuan et al., 2022) respectively used a magnetic TENG and metamaterial-inspired TENG as a self-power motion monitoring sensor and power source for a vibration monitoring system.

To the best of our knowledge, there is currently no literature for studying the fault diagnosis of TENG. Nevertheless, progress has been made in the field of the fault diagnosis of conventional generators. Yang et al. (Yang, Chai, Yin, & Tao, 2018) established a linear parameter varying model by incorporating the electromechanical dynamics into the current dynamics and realized the current sensor fault diagnosis for a permanent magnet synchronous generator (PMSG). Considering that detailed mechanism knowledge is required for the model-based fault diagnosis method (Liang, Zhang, Al-Durra, Muyeen, & Zhou, 2022; Lin, Xu, & Ye, 2021), and the collected signals also contain sufficient fault signatures, Xu et al. (Xu, Tao, et al., 2022) realized the fault diagnosis of back-to-back converters in PMSG wind turbine systems based on the instantaneous current amplitude, and Chen et al. (Chen, He, & Sui, 2021) developed a fault diagnosis method for the open-switch of three-level rectifiers based on selective calculation method for instant voltage deviation. To cope with the problem that the collected signals are susceptible to background noise, Gao et al. (Gao, Feng, & Liang, 2021) realized a data-driven planetary gearbox fault diagnosis framework for wind turbines by analyzing three kinds of spectrums of stator current signals generated by PMSG. Moreover, Ali et al. (Ali et al., 2021) developed a machine learning-based fault diagnosis method for the open switch of cascade H-bridge multi-level inverter based on the combination of the probability principal component analysis and support vector machine. However, the selection of fault extractors and classifiers for traditional data-driven fault diagnosis methods significantly relies on artificial experience. Aiming to overcome the limitations of traditional data-driven fault diagnosis methods, deep learning methods have been developed rapidly recently in the field of electrical machinery fault diagnosis. Xue et al. (Xue, Li, Xiahou, Ji, & Wu, 2019; Xue, Xiahou, Li, Ji, & Wu, 2020) successively developed a convolutional neural network (CNN) and long short-term memory network for the fault diagnosis of the open-circuit switch of the back-to-back converter in wind generation systems. Thereafter, Gong et al. (Gong, Chen, Zhang, Zhang, & Gao, 2020) developed a fault diagnosis method for electrical power DC-DC inverter based on an improved CNN.

The reasons for the wide application of deep learning-based fault diagnosis methods in the field of conventional electrical machinery can be explained as follows. The operating process of power-switching devices in electrical machinery presents nonlinear and time-varying characteristics, resulting in there exist a nonlinear relationship between the device status and the collected signals (Liang et al., 2022). As an intelligent data-driven method, deep learning methods can express the nonlinear relationship by analyzing the signal characterizing the device status (Lin & Xu, 2023). Besides, the characteristics of adaptively feature extraction and fault identification for deep learning methods reduce the dependence of diagnosis performance on artificial experience (Liang et al., 2022).

Considering that there exists a nonlinear relationship between the status of TENG and the voltage signals due to the relative motion of the positive/negative triboelectric layers (Lone et al., 2022), and inspired by the promising fault diagnosis performance of deep learning methods in the field of conventional electrical machinery, a novel deep learning framework based on attention neural network (AttCNN) is proposed in this study for the fault diagnosis of TENG. The global correlation features in voltage signals extracted by the attention mechanism in AttCNN can effectively reflect the status variation of TENG among different moments, and the feature information extracted by the convolutional network in AttCNN guarantees the fault diagnosis efficiency of TENG. Thereby the proposed method fills in the gaps in the field of fault diagnosis for TENG, which contributes to the safe and high-efficiency operation of TENG.

The rest of this study is organized as follows. In Section 2, the processes of establishing the experimental TENG and data acquisition are described. Section 3 describes the proposed fault diagnosis methodology based on AttCNN. Section 4 implements the sensitivity analysis and generalization evaluation of the proposed fault diagnosis methodology, and the performance comparison between the proposed method and previous data-driven methods is also presented in this section. Finally, conclusions are drawn in Section 5.

2. Test bench of a TENG and data acquisition

2.1. Establishment of TENG

In this study, an improved TENG was established, and the experimental devices for fabricating TENG are depicted in Fig. 1. Moreover, the movement of devices attached by TENG is demonstrated in Fig. 2. As shown in Fig. 1 and Fig. 2, the positive/negative triboelectric layers were stacked in Board-I and Board-III, respectively, Board-III can be moved back and forth on Board-II to adjust the initial distance between the positive and negative triboelectric layers, and the shaker is capable of producing periodic shakes that make negative triboelectric layer contact with positive triboelectric layer periodically. In terms of materials for fabricating TENG, the material of the three boards is aluminum (Al), nickel cloth (Nc) was used as electrodes, polyamide (PA) and polytetrafluoroethylene (PTFE) were used as the positive and negative triboelectric layers, respectively, and graphite paper (Gp) and polyimide (PI) were used as interlayers. As referred from Ref. (Chun et al., 2016), the strategy of embedding an interlayer between the triboelectric layer and electrode is conducive to reducing charge diffusion, thereby improving the output performance of TENG.

As Ref. (Lee et al., 2017) indicated that a soft substrate can increase the contact area of the two triboelectric layers, and considering that the experimental devices (three boards made of Al) may interfere with the electric output, a 2 mm thick sponge and 0.15 mm thick PI layer were

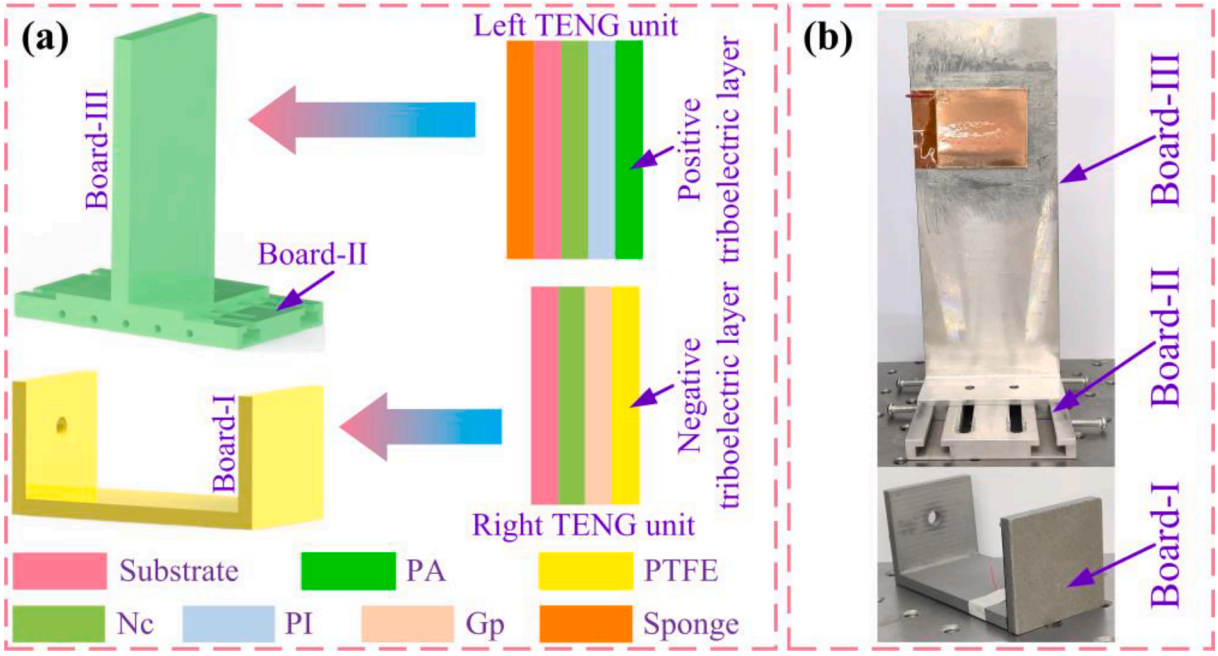

Fig. 1. The experimental device of TENG: (a) the detailed schematic of TENG; (b) the real experimental device.

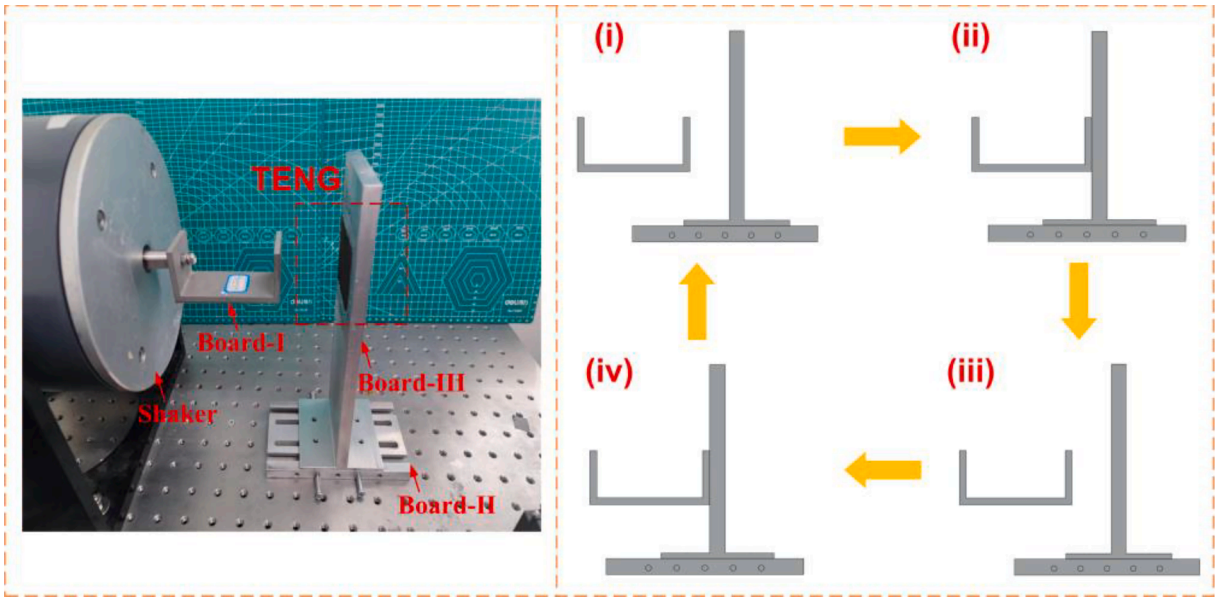

Fig. 2. The movement diagram of boards attached by TENG.

used as a buffer layer and substrate, respectively. Therein, the sponge was made of polyurethane with a par per inch of 60. Besides, the sizes of the positive/negative triboelectric layers and interlayers are 40 mm × 40 mm, and the size of the two electrodes is 50 mm × 40 mm. Note that the size of electrodes is larger than that of triboelectric layers or interlayers, which is to avoid the influence of wires on the contact area of positive/negative triboelectric layers.

The working principle of the established TENG is shown in Fig. 3. Notably, the interlayers are not presented in Fig. 3 for simplification. According to the effect of triboelectrification and electrostatic induction, with the contact of positive/negative triboelectric layers, numerous positive/negative charges accumulate on the surfaces of the positive/negative triboelectric layers, respectively. As the two triboelectric layers move away from each other, the two electrodes induce positive/negative charges, respectively, and a current flows from the bottom electrode to the top electrode as shown in Fig. 3(b). While the two triboelectric layers separate to a certain distance, the two electrodes reach an electrostatic equilibrium state as shown in Fig. 3(c). And then, as the two triboelectric layers move towards again, the electrostatic balance between the two electrodes is broken, and a current flows from the top electrode to the bottom electrode is generated. Finally, while the two triboelectric layers contact again, the two electrodes restore electrostatic balance.

2.2. Test bench for data acquisition

In this study, a deep learning method is proposed for the fault diagnosis of TENG. As an intelligent data-driven method, the good fault

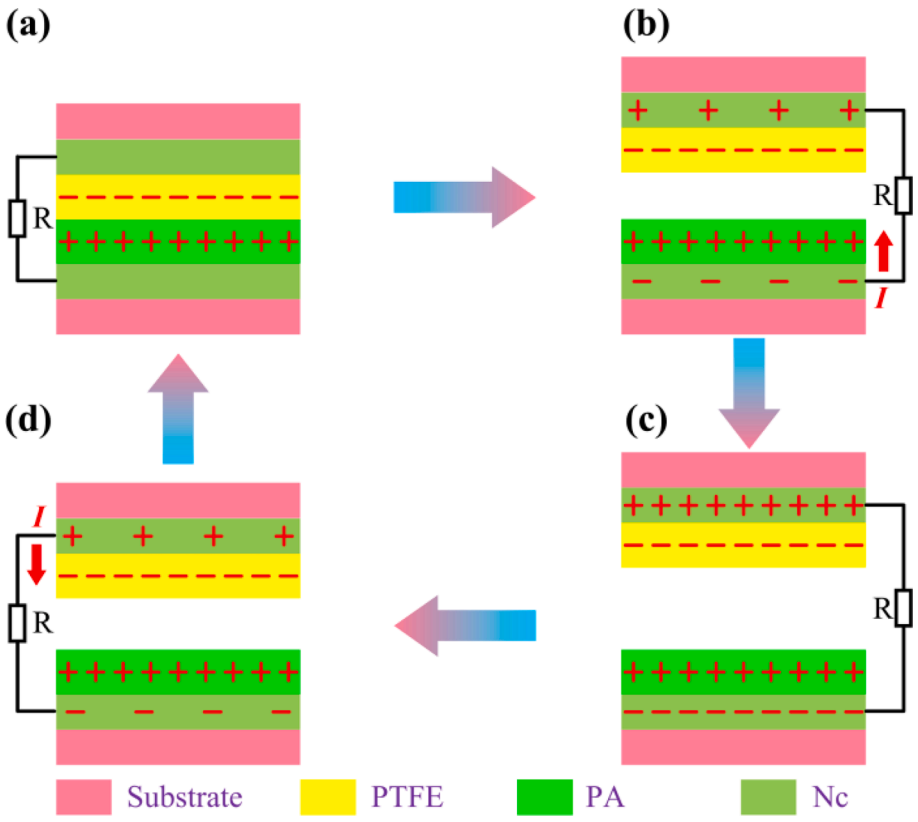

Fig. 3. The working principle of TENG.

diagnosis performance of the proposed method relies on a large amount of data reflecting the operating status of TENG (Liang et al., 2022). The voltage signal, as the output signal of TENG, contains sufficient information reflecting the operating status of TENG (Liang et al., 2022; Lone et al., 2022). Aiming to excite the TENG to generate voltage signals, a test bench was built in Fig. 4(a).

As depicted in Fig. 4(a), the test bench mainly consists of a PC, controller (Econ VT-9002), power amplifier (Econ E5874A), and shaker (Econ E-JZK-50). Therein, the Board-I and Board-II shown in Fig. 1 were connected to the shaker and a fixed platform with screws, respectively, and the initial distance between the positive triboelectric layer (stacked in Board-I) and the negative triboelectric layer (stacked in Board-III) was 2 mm, and then, the excitation generated by the shaker can drive a periodic contact between the positive/negative triboelectric layers. Notably, to suppress the interference from environmental vibration, the entire test bench was placed on a vibration-isolation platform.

According to the working principle of TENG described in Section 2.1, charges are generated in the operating process of the test bench. Aiming to measure the electric parameters, the established measuring circuits are depicted in Fig. 4(b). Therein, the short-circuit currents and transferred charges were measured by an electrometer (Keithley 6514), and the output voltage of TENG was measured by an oscilloscope (Tektronix MDO3024). Moreover, the room temperature and humidity were measured by a commercial thermo-hygrometer (JR916).

2.3. Data acquisition

As described in Section 2.1, the addition of interlayers is conducive to improving the output performance of TENG. While with the increase in hours of service, the thickness of interlayers (*TI*) gradually changes. As referred from Ref. (Xin et al., 2022), the variation in *TI* has a significant impact on the output performance of TENG. In addition to the interlayers, the contact frequency (*CF*) of the positive/negative triboelectric layer is also a factor affecting the output performance of TENG (Xin et al., 2022). Since the decline of the output performance of TENG may increase the usage cost and even endanger the users (Yuan et al., 2022; Zhao, Liu, et al., 2022), timely condition monitoring and fault diagnosis for TENG is significant.

To explore the effectiveness of the proposed deep learning framework for the fault diagnosis of TENG, and considering that a timely fault diagnosis can effectively suppress the further deterioration of the failure, the fault diagnosis performance of the proposed method in single fault (*TI* or *CF*) is evaluated in this study. As Section 2.2 described that the output voltage signals contain sufficient feature information reflecting the status of TENG, the voltage signals under different operating conditions need to be collected to provide data support for the fault diagnosis of TENG.

On the basis of the established test bench in Section 2.2, the voltage signals of TENG under different operating conditions can be generated. In the experiments, the TENG with $CF = 6$ Hz and $TI = 0.15$ mm is supposed to be the healthy TENG, and different cases of *CF* and *TI* correspond to different fault statuses. The values of *CF* and *TI* for different fault labels of TENG are tabulated in Table 1.

In the process of collecting the voltage signals under different fault labels, the sampling frequency and sampling time of the oscilloscope were set as 5000 Hz and 200 s, respectively. With the experiment, a total of 7 groups of voltage sequences corresponding to the 7 fault labels in Table 1 were obtained, and the sequence length of each group of sequences is 1000000. Fig. 5 depicts the voltage signals within [99 s, 99.5 s] for different fault labels. With the comparison of voltage signals under different fault labels depicted in Fig. 5, a brief analysis of the failure mechanism of TENG is described as follows. In different fault cases, the voltage output changes due to the change of charge. As the frequency of external force increases, the charge transfer rate increases, and the amount of charge per unit time increases, which makes the amplitude of voltage increase with *CF* increase. The property of PI material affects charge trapping sites. The amount of charge transfer varies with the conditions of trapping sites. This makes the voltage amplitude change

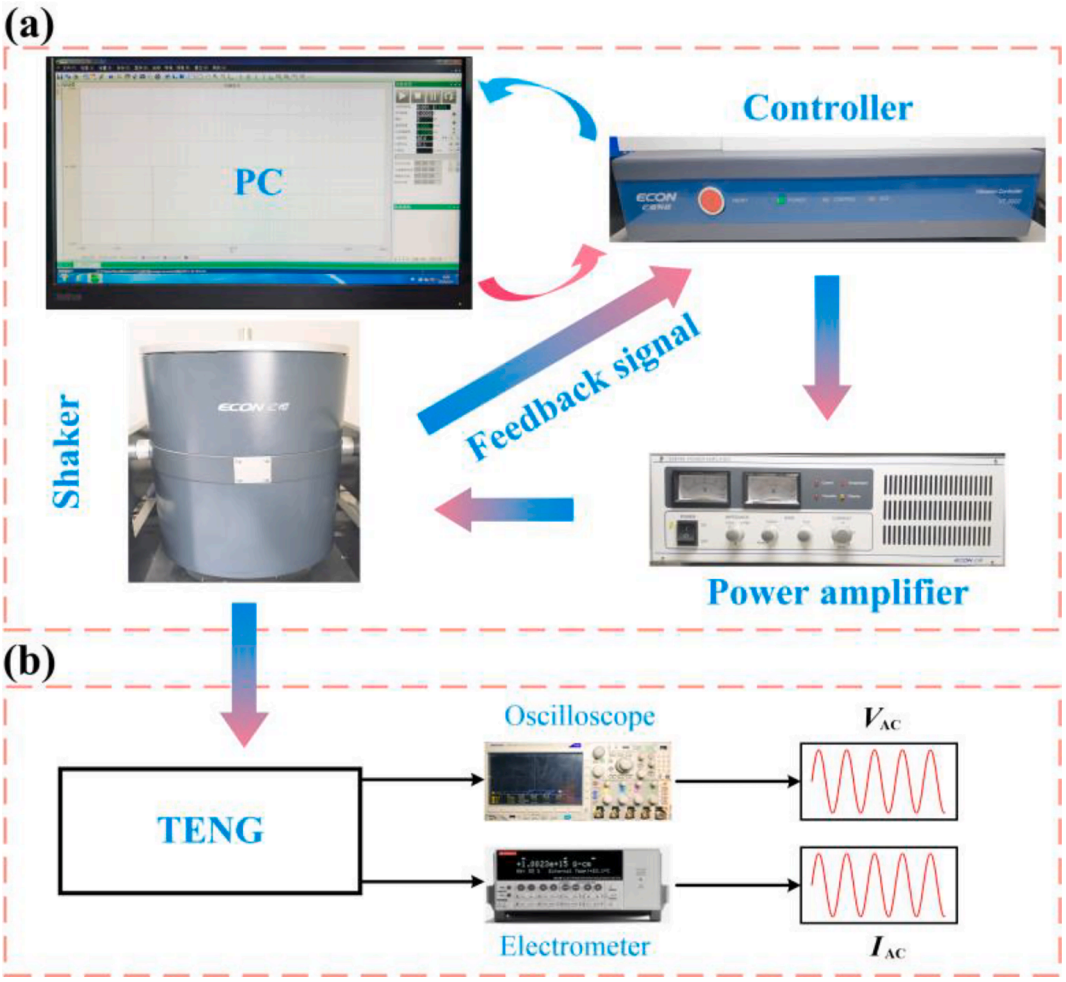

Fig. 4. Test bench for exciting TENG to generate voltage signals: (a) test bench; (b) the measuring circuits.

Table 1
Details for different fault labels of TENG.

Fault item	*CF* (Hz)	*TI* (mm)	*Label*
Health	6	0.15	0
Fault_CF_1	4	0.15	1
Fault_CF_2	8	0.15	2
Fault_TI_1	6	0.125	3
Fault_TI_2	6	0.1	4
Fault_TI_3	6	0.075	5
Fault_TI_4	6	0.05	6

with different *TI* conditions. The increase of *TI* provides a wider range of charge trapping sites, which improves the charge transfer efficiency. This makes the voltage amplitude increase with the increase of *TI*.

3. Methodology

3.1. Formulation for the fault diagnosis of TENG

As referred from Refs. (Lei et al., 2020; Liang et al., 2022), there exists a mapping relationship between the status of TENG and collected voltage signals. The process of implementing fault diagnosis for TENG is to establish this mapping relationship. In general, the mapping relationship can be expressed as

$$s = F(V) \tag{1}$$

where *s* and *v* represent the status of TENG and collected voltage signals, respectively.

3.2. Establishment of AttCNN

The mapping relationship *F* also presents a nonlinear characteristic, because there exists a nonlinear relationship between the status of TENG and the voltage signals due to the relative motion of the positive/negative triboelectric layers (Lone et al., 2022). Considering that sufficient feature information reflecting the status of TENG is contained in the collected voltage signals (Zhang et al., 2022), a deep learning method is used to establish the nonlinear relationship *F* by analyzing the collected voltage signals.

According to the characteristic of TENG, aiming to extract the feature information reflecting the status of TENG more comprehensively, a novel deep learning framework, AttCNN, is proposed in this study. The framework of AttCNN is depicted in Fig. 6, it shows that AttCNN is mainly composed of an attention block, convolutional block, and classified block. In the following, the motivation for the application of each block is briefly described.

3.2.1. Attention block

The voltage signal collected from TENG is generally a signal sequence, and the relative motion of the positive/negative triboelectric layers is approximately periodic, so, the status of TENG is difficult to be directly identified by analyzing the voltage signal at certain moments. Besides, considering that the fault of TENG is generally evolutionary, the analysis of a long-term voltage signal sequence is significant for the fault diagnosis of TENG, because the extracted feature information can reflect

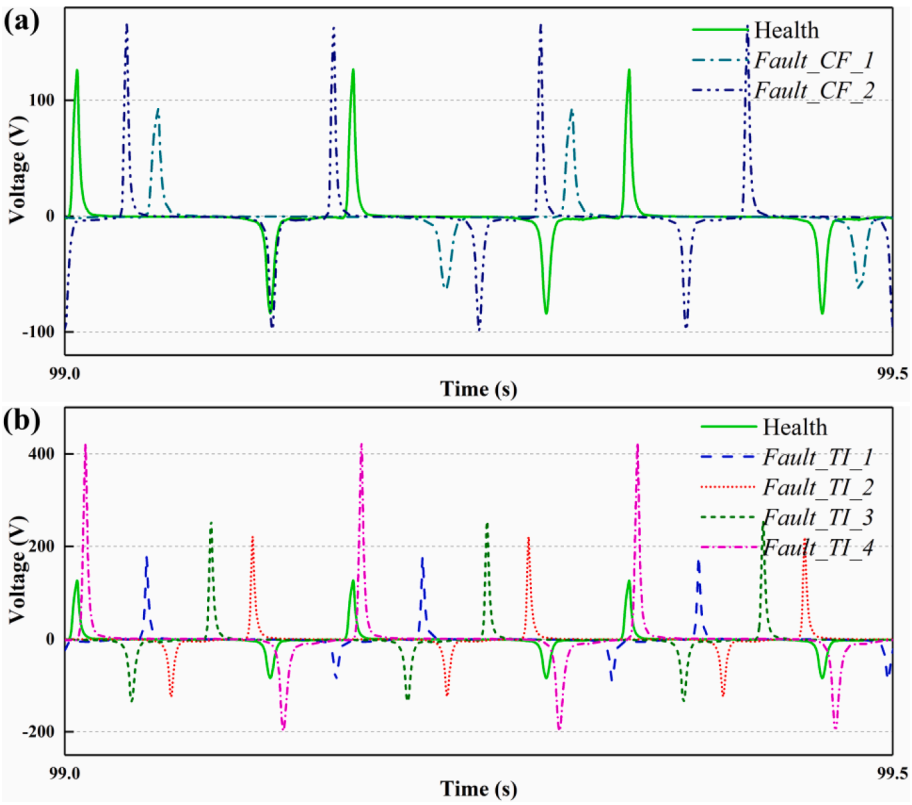

Fig. 5. The collected voltage signals under different fault labels: (a) comparison of voltage signals under health status and two cases of *CF*; (b) comparison of voltage signals under health status and four cases of *TI*.

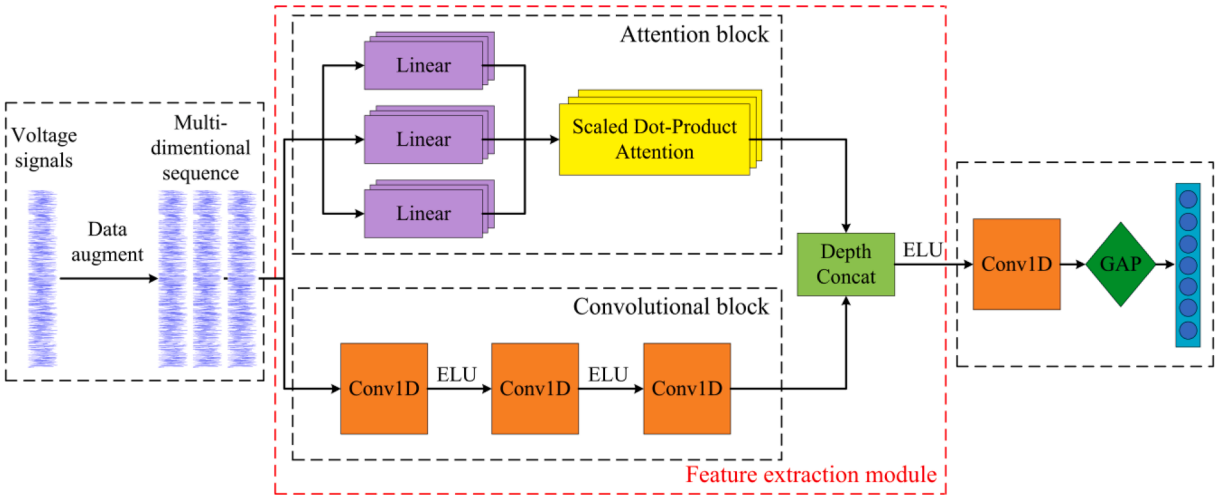

Fig. 6. The framework of AttCNN.

the status variation of TENG among different moments. As inferred from the application of the Transformer in natural language processing (Vaswani, Shazeer, Parmar, Uszkoreit, Jones, Gomez, Kaiser, & Polosukhin, 2017), the distance of positions between any two moments in a signal sequence can be converted into 1 with the attention mechanism. Thus, an attention block is applied in AttCNN.

The structure of the attention block is depicted in Fig. 7. It shows that a multi-head attention structure is applied in the attention block, and the attention mechanism used in each attention head is the scaled dot-product attention. The mathematical expression of the attention block is

$$\mathrm{MhAtt}(X) = \mathrm{Concat}(head_1, head_1, \ldots, head_{n\_h})W_O \tag{2}$$

where MhAtt(X) is the output of the attention block, Concat denotes the operation of concatenating multiple attention heads at the feature dimension, and n_h denotes the number of the attention head. $head_i$ is the i-th attention head, and its expression is

$$head_i\text{: Attention}(Q^{(i)}, K^{(i)}, V^{(i)}) = \mathrm{softmax}\left(\frac{Q^{(i)}\left(K^{(i)}\right)^{\mathrm{T}}}{\sqrt{d_K}}\right)V^{(i)} \tag{3}$$

where $Q^{(i)}$, $K^{(i)}$, and $V^{(i)}$ are the linear mapping of the input matrix X, respectively, and the linear mapping matrics are $W_Q^{(i)} \in \boldsymbol{R}^{d_m \times d_K}$, $W_K^{(i)} \in \boldsymbol{R}^{d_m \times d_K}$, and $W_V^{(i)} \in \boldsymbol{R}^{d_m \times d_K}$, respectively. d_m represents the feature

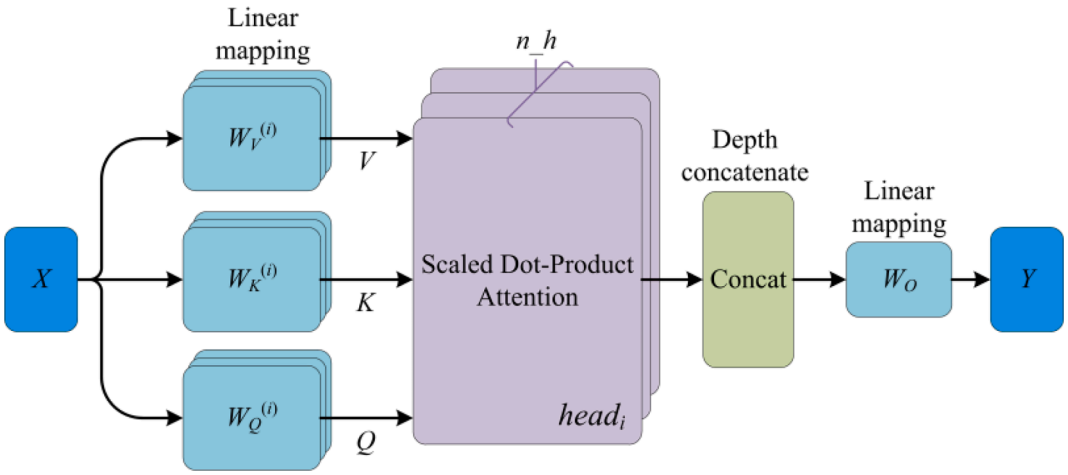

Fig. 7. The structure of the attention block.

dimension of X and $d_K = d_m/n\_h$. Besides, the expression of the softmax function is

$$\mathrm{softmax}(z^{(i)}) = \frac{\exp(z^{(i)})}{\sum_{i=1}^{n\_h}\exp(z^{(i)})} \tag{4}$$

With multi-head attention, AttCNN can extract fault information from the feature subspace of voltage signals, thereby reflecting the status of TENG more comprehensively (Vaswani et al., 2017). Moreover, the computational cost of multi-head attention is similar to that of single-head attention, and parallel computing is supported for the training of multi-head attention, so, AttCNN possesses a good training efficiency with the assistance of GPU acceleration. Remarkably, a python platform built with NVIDIA GeForce RTX 3090 and TensorFlow framework was applied in this study for the training of AttCNN.

3.2.2. *Convolutional block*

Although the attention mechanism can extract the global correlation features of sequences, the lack of inductive bias ability makes it difficult to be trained. As convolutional layers introduce the inductive bias (Ajit, Acharya, & Samanta, 2020; Jiao, Zhao, Lin, & Liang, 2020), the local features contained in voltage signals can be effectively extracted, which makes up for the deficiency of the attention mechanism (Bello, Zoph, Le, Vaswani, & Shlens, 2019). Hence, aiming to improve the efficiency of fault diagnosis for TENG, convolutional layers are added in AttCNN.

The information flow in convolutional layers can be expressed as

$$y^{(l)} = f(y^{(l-1)} * W^{(l)} + b^{(l)}) \tag{5}$$

where $y^{(l)}$ represents the output of the l-th convolutional layer, and $W^{(l)}$ and $b^{(l)}$ are weights and biases in the l-th convolutional layer, respectively. * represents the convolution operation, and the principle of convolution operation is depicted in Fig. 8. It shows that the convolution operation in convolutional layers is an element-wise product of the filter and the receptive field in the input. Besides, f represents the activation function. As referred from Ref. (Goodfellow, Bengio, & Courville, 2016), as an activation function, exponential linear units (ELU) not only alleviate the problem of gradient propagation anomy but also make the output of network layers close to a zero-center distribution. Thereby the application of ELU is conducive to the improvement of the training efficiency of networks (LeCun, Bottou, Orr, & Müller, 2012; Wiesler & Ney, 2011). Thus, ELU is adopted as the activation function in AttCNN, and the expression of the applied ELU in this study is as Eq. (6).

$$y = \begin{cases} \exp(x) - 1, x \leqslant 0 \\ x\ , x > 0 \end{cases} \tag{6}$$

3.2.3. *Classified block*

With the attention block and convolutional block, the feature information that reflects the status of TENG is extracted. Aiming to realize the nonlinear relationship F in Eq. (1), a mapping between the status of TENG and the extracted feature information is required.

As referred from Refs. (Li, Li, Xu, Xiong, & Gao, 2018; Lin, Chen, & Yan, 2014), global average pooling (GAP) layers and fully connected (FC) layers are generally used for establishing the mapping between the label and extracted features. To compare the performance of GAP layers

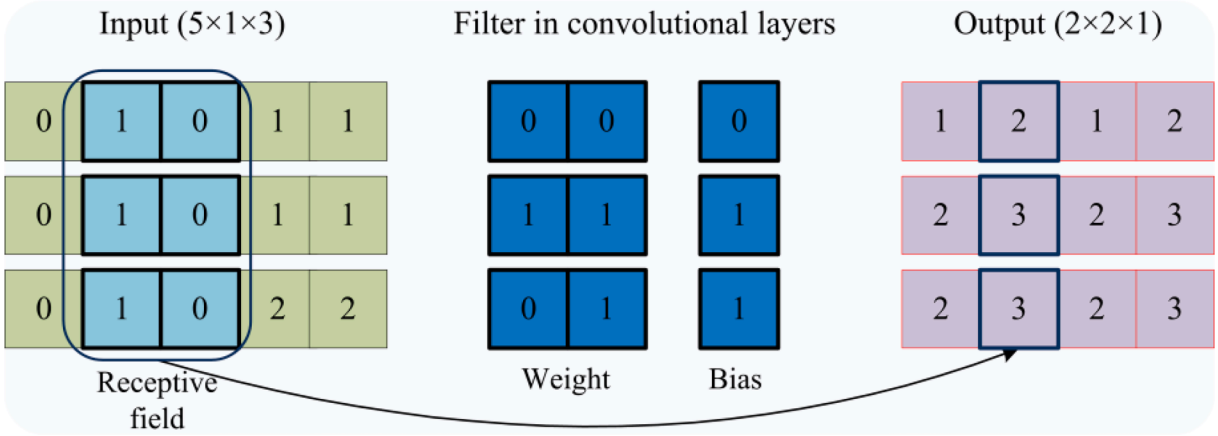

Fig. 8. The principle of convolution operation in convolutional layers.

and FC layers in establishing the mapping, a comparative study was performed. The results indicated that the status identification accuracies under the cases of GAP layers and FC layers were very close, while the scale of training parameters of FC layers was significantly larger than that of GAP layers, thus, the GAP layer is applied in AttCNN for establishing the mapping between the status of TENG and the extracted feature information.

3.2.4. Parameters of AttCNN

The specific parameters of AttCNN are tabulated in Table 2. Notably, Table 2 only lists an AttCNN architecture with a specific hyperparameter setting. To guarantee the fault diagnosis performance of AttCNN, the hyperparameters require to be fine-tuned according to practical applications.

3.3. Framework for the fault diagnosis of TENG

On the basis of the proposed AttCNN, the framework for the fault diagnosis of TENG is shown in Fig. 9. It shows that there exist three steps: data collection and processing, offline training of AttCNN, and online fault diagnosis of TENG. The details of each step are as follows:

(i) Data collection and processing. The voltage signals collected from TENG are classified into two groups: historical and real-time voltage signals, which are used for training AttCNN and performing online fault diagnosis, respectively. Since there may exist outliers in collected voltage signals, and the length of two collected voltage signal sequences may be different, the operation of data processing is implemented. The details of data processing are depicted in Fig. 10.

(ii) Offline training of AttCNN. With the processed historical voltage signals, the sample sets (training, validation, and testing sets) are obtained through data division, and the details are tabulated in Table 3. Subsequently, based on the sample sets, AttCNN is trained through the back-propagation algorithm (Rumelhart, Hinton, & Williams, 1986). The details of network training can be found in Ref. (Y. Lin & Xu, 2023).

(iii) Online fault diagnosis of TENG. Based on the optimal trained AttCNN in step (ii), the online fault diagnosis of TENG can be performed with the processed real-time voltage signals as the input of AttCNN. Finally, the output of AttCNN is the predicted status of TENG.

4. Results and discussion

4.1. Influence of hyperparameters on fault diagnosis performance

On the basis of the sample sets (the training, validation, and testing sets) tabulated in Table 3, the fault diagnosis performance of the proposed AttCNN is evaluated in this subsection. According to Ref. (Goodfellow et al., 2016), the fault diagnosis performance of AttCNN can be optimized by training the learnable parameters (weights and biases) of AttCNN. Nevertheless, Ref. (L. Yang & Shami, 2020) also indicated that the fault diagnosis performance of AttCNN is affected by the hyperparameters of AttCNN. So, the sensitivity analysis of hyperparameters on the performance of AttCNN for the fault diagnosis of TENG is implemented.

4.1.1. Number of attention heads

As inferred from Section 3.2, with the application of multi-head attention, AttCNN can effectively extract global correlation fault features from the voltage signal collected from TENG, which reflects the status variation of TENG at different moments. Since the number of attention heads (n_h) can affect the ability of multi-head attention in extracting fault features from the feature subspace of voltage signals, the fault diagnosis performance of AttCNN may be influenced by the value of n_h.

Aiming to analyze the influence of the hyperparameter n_h on the fault diagnosis performance of AttCNN, the fault diagnosis results of AttCNN with different cases of n_h are compared. According to the information tabulated in Table 2, based on the datasets described in Table 3, the input format of the attention block is $\boldsymbol{R}^{720\times12}$. Aiming to satisfy the principle that n_h and the feature dimension of each attention head (*size_per_head*) are integers, the recommended value range of n_h is {2, 3, 4, 6}. Notably, to follow the variable-controlling method, the other hyperparameters of AttCNN are consistent with those tabulated in Table 2, and the batchsize and maximum epoch are set as 128 and 2000, respectively.

On the basis of the training and validation sets described in Table 3, the training processes of AttCNN under different cases of n_h are depicted in Fig. 11. Since the purpose of the sensitivity study is to show the difference in fault diagnosis results under different hyperparameters intuitively, only the results under three cases of n_h are shown in Fig. 11 for simplification (Y. Lin & Xu, 2023). As depicted in Fig. 11(a), the convergence efficiency of fault diagnosis accuracy on the training set is improved with the increase of n_h. While on the validation set, the fault diagnosis accuracy under $n\_h = 4$ or $n\_h = 6$ is not as stable as that under $n\_h = 2$. The reasons for this phenomenon can be explained as follow. The role of the validation set is to tentatively evaluate the generalization performance of AttCNN trained by the training set. As the feature subspace of voltage signals is reduced with the increase of n_h, the feature information extracted by AttCNN is insufficient to completely characterize the status of TENG. So, the stability of the fault diagnosis accuracy on the validation set may be reduced with the increase of n_h. Besides, the relatively small feature dimension of the dataset used in this study is also a reason that induces the phenomenon in Fig. 11(b).

Aiming to further evaluate the performance of AttCNN under different cases of n_h, the convergence performance of fault diagnosis accuracy on the validation set is compared. The convergence value and convergence epoch of fault diagnosis accuracy under different cases of n_h are depicted in Fig. 12(a). Therein, the definition of convergence value and convergence epoch is as follows. If the training process is convergent, the average value of accuracy within the range of (1800, 2000] in Fig. 11 is considered the convergence value of the fault diagnosis accuracy. Besides, the convergence epoch is considered as the epoch where the average value of accuracy within the previous 50 consecutive epochs is greater than the convergence value.

As depicted in Fig. 12(a), the performance of AttCNN under $n\_h = 2$ is

Table 2
Parameters of AttCNN.

Layer	Sub_block	Sub_layer type	Kernel size	Output (Len_seq, Depth)
Input				720, 1
Convolution		Conv1D		720, 12
Feature extraction module	Attention block	Attention		720, 12
	Convolutional block	Conv1D + ELU	1 × 1	720, 32
		Conv1D + ELU	3 × 3	720, 64
		Conv1D	1 × 1	720, 12
	Depth Concat	Concatenate + ELU		720, 24
Convolution		Conv1D	1 × 1	720, 7
GAP		GlobalAveragePooling1D		1, 7
Output		Softmax		1,7

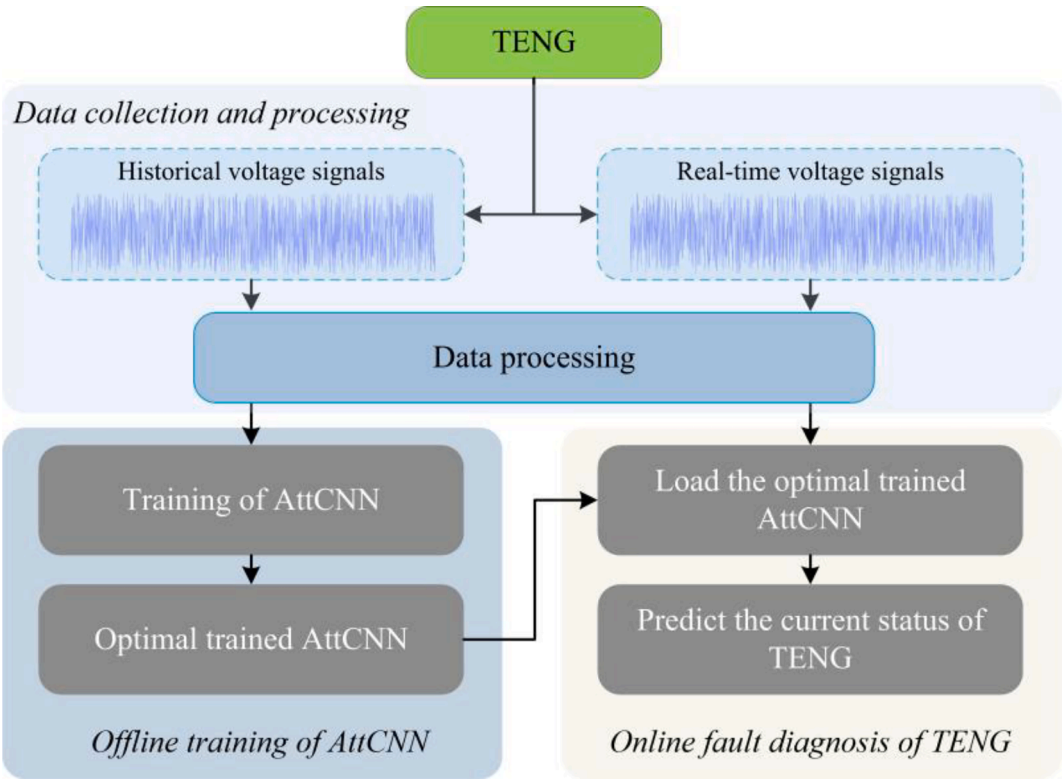

Fig. 9. Framework for the fault diagnosis of TENG.

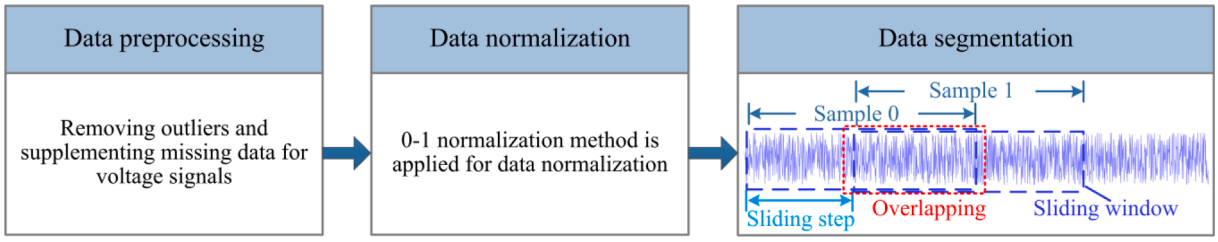

Fig. 10. The operation of data processing. *The principle of identifying the outliers and missing data of signals can be found in Ref. (Cheliotis, Gkerekos, Lazakis, & Theotokatos, 2019).

Table 3
Details of data division.

Data set	Proportion	Number of samples	Role
Training set	70%	13,601	Learn the trainable parameters of AttCNN
Validation set	20%	3885	Evaluate the generalization performance of AttCNN tentatively in the training process
Testing set	10%	1946	Evaluate the fault diagnosis accuracy and generalization performance of the trained AttCNN

better than that under $n\_h = 4$ or $n\_h = 6$ in terms of the convergence epoch and convergence values of fault diagnosis accuracy. Besides, a metric *Dev* is introduced to quantify the stability of the convergence results of AttCNN under different cases of n_h, and the expression of *Dev* is

$$Dev = \mathrm{sqrt}(\mathrm{abs}(Acc - C\_Acc)) \tag{7}$$

where *Acc* and *C_Acc* represent the fault diagnosis accuracy at an epoch and the convergence value, respectively. The comparison of *Dev* under different cases of n_h is depicted in Fig. 12(b). As indicated in Fig. 12(b), the stability of the convergence results of AttCNN under $n\_h = 2$ is better than that under $n\_h = 4$ or $n\_h = 6$.

Hence, according to the results in Fig. 11 and Fig. 12, the hyper-parameter n_h has a certain impact on the fault diagnosis performance for TENG. Moreover, in respect of the convergence results on the validation set, the AttCNN with $n\_h = 2$ possesses the best fault diagnosis performance for TENG.

4.1.2. Learning rate

As referred from Ref. (Goodfellow et al., 2016), the value of learning rate (*lr*) generally has a significant impact on the performance of neural networks. So, the fault diagnosis results of AttCNN on the training and validation sets under different cases of *lr* are compared in this subsection.

According to the description in Refs. (Goodfellow et al., 2016; Hinton, 2012), an approximate logarithmic scale is generally recommended for the value range of the hyperparameter *lr*. So, the recommended value range of *lr* is {1e-4, 5e-4, 1e-3, 5e-3, 1e-2, 5e-2, 1e-1} in this study. As Section 4.1.1 indicated that the AttCNN with $n\_h = 2$ possesses a better fault diagnosis performance, only the fault diagnosis results of AttCNN

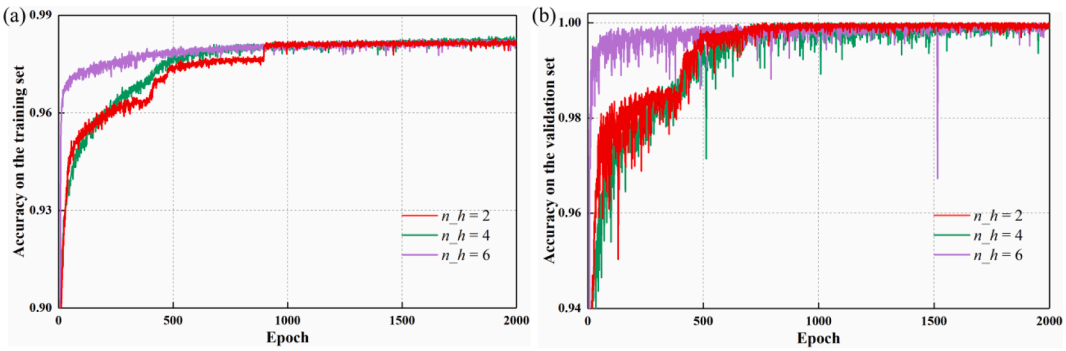

Fig. 11. Training processes of AttCNN under different cases of *n_h*: (a) the accuracy on the training set; (b) the accuracy on the validation set.

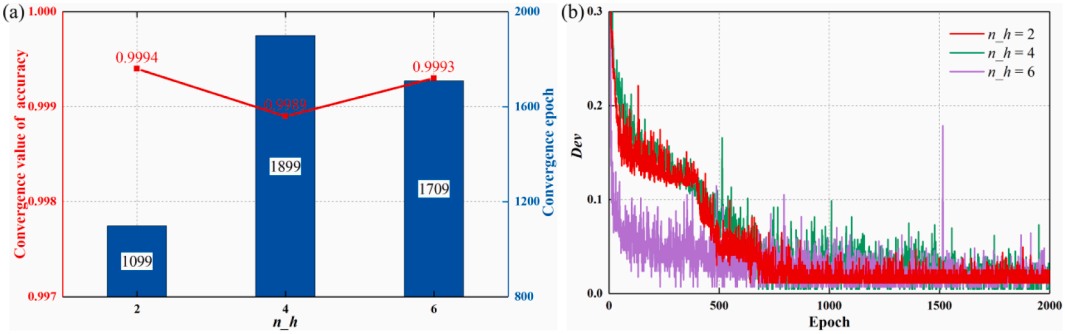

Fig. 12. The convergence results of AttCNN on the validation set under different cases of *n_h*: (a) the convergence results of the fault diagnosis accuracy; (b) the results of *Dev*.

with $n\_h = 2$ under different cases of *lr* are compared for simplification.

Similar to Section 4.1.1, aiming to intuitively present the influence of *lr* on the fault diagnosis performance of AttCNN, the training processes of AttCNN on the training and validation sets under three cases of *lr* are depicted in Fig. 13. As indicated in Fig. 13(a) and (b), there exists a similar trend for the fault diagnosis accuracies on the training and validation sets. Therein, the fault diagnosis accuracy of AttCNN on the training or validation sets under the case of $lr = 1e\text{-}3$ is obviously better than that under two cases of $lr = 1e\text{-}4$ and $lr = 5e\text{-}2$. Moreover, the result under $lr = 5e\text{-}2$ reveals that a relatively large value of *lr* may result in difficulty for the convergence of fault diagnosis accuracy.

Aiming to further compare the convergence performance of AttCNN under two cases of $lr = 1e\text{-}3$ and $lr = 1e\text{-}4$, the convergence results of AttCNN on the validation set under two cases of *lr* are depicted in Fig. 14. As indicated in Fig. 14(a), the performance of AttCNN under the case of $lr = 1e\text{-}3$ is better than that under $lr = 1e\text{-}4$ in terms of the convergence value and convergence epoch. Moreover, the results of *Dev* in Fig. 14(b) further validate that the fault diagnosis performance of AttCNN under $lr = 1e\text{-}3$ is better than that under $lr = 1e\text{-}4$.

Hence, the results in Fig. 13 and Fig. 14 reveal that the AttCNN with $lr = 1e\text{-}3$ possesses the best fault diagnosis performance on the training and validation sets. The reasons that there exist deviations in fault diagnosis performance between different cases of *lr* can be explained as follows. An excessively large value of *lr* may cause the training results of AttCNN difficult to be converged, resulting in an unstable training process as Fig. 13(a) and (b); while an excessively small value of *lr* may cause the trainable parameters to fall into a local optimum, thereby delaying the convergence of AttCNN (Goodfellow et al., 2016).

According to the results in Section 4.1.1 and Section 4.1.2, the hyperparameters of *n_h* and *lr* have a significant impact on the fault diagnosis performance for TENG. Hence, the hyperparameters of AttCNN should be fine-tuned in practical applications.

4.2. Evaluation of the generalization performance of AttCNN

Considering that a timely fault diagnosis is important for the safe operation of TENG, it is necessary to be able to use the proposed AttCNN for the real-time fault diagnosis of TENG. As the generalization

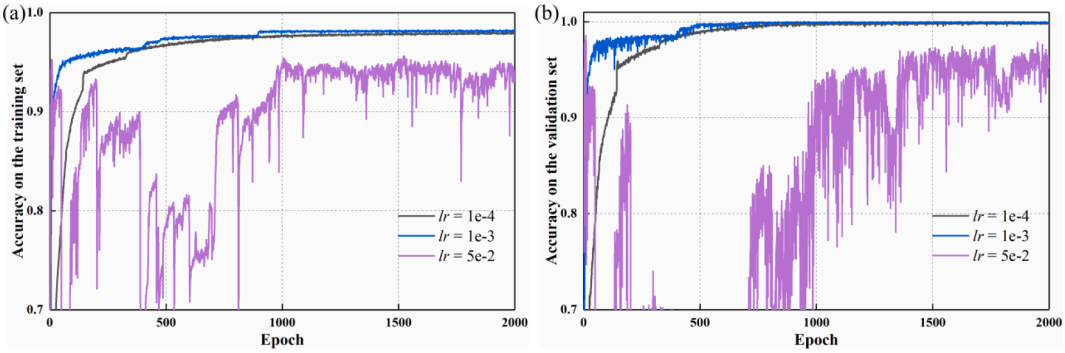

Fig. 13. Training processes of AttCNN under different cases of *lr*: (a) the accuracy on the training set; (b) the accuracy on the validation set.

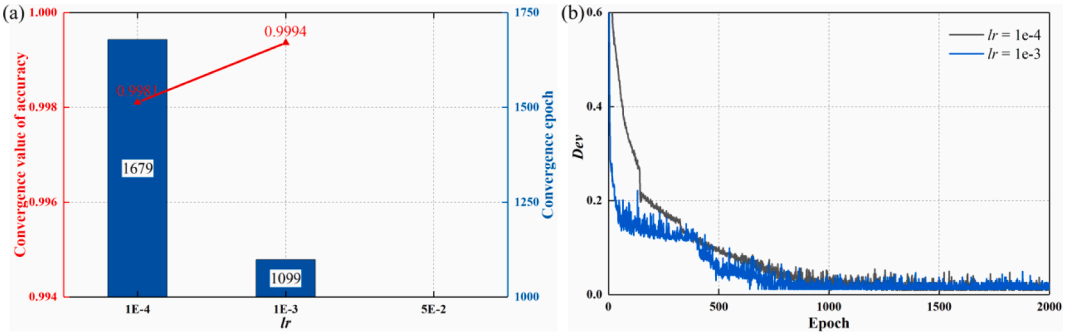

Fig. 14. The convergence results of AttCNN on the validation set under different cases of *lr*: (a) the convergence results of the accuracy; (b) the results of *Dev*.

performance can effectively reflect the capability of AttCNN for real-time fault diagnosis, the generalization performance of AttCNN for the fault diagnosis of TENG is evaluated in this subsection.

As tabulated in Table 3 of Section 3.3, the testing set is independent of the training and validation sets. Since the testing set does not participate in the training process of AttCNN, the fault diagnosis results on the testing set can be used for evaluating the generalization performance of AttCNN. As the results in Section 4.1 indicated that the trained AttCNN with $n\_h = 2$ and lr = 1e-3 possesses the best fault diagnosis performance, it is selected to evaluate the generalization performance of AttCNN in this subsection.

The fault diagnosis result of the trained AttCNN on the testing set is depicted in Fig. 15, and the corresponding fault diagnosis accuracy for different fault labels is tabulated in Table 4. As indicated in Fig. 15 and Table 4, the overall fault diagnosis accuracy of the trained AttCNN on the testing set is 99.59%. Moreover, except for a few samples corresponding to *Label* 0 and *Label* 1, the trained AttCNN realizes a correct diagnosis for other samples. Nevertheless, the fault diagnosis accuracy of the AttCNN for all fault labels is greater than 97.84%. As referred from Refs. (Li, Pan, & Huang, 2019; Lin & Xu, 2023; Qin et al., 2021), a fault diagnosis accuracy that exceeds 95% is generally considered acceptable in engineering.

Hence, according to the results in Fig. 15 and Table 4, for the testing set, the predicted fault labels of the trained AttCNN and the actual fault labels are in good agreement. Since AttCNN is trained with the training and validation sets, the fault diagnosis result on the testing set indicates that AttCNN possesses a promising generalization performance for the fault diagnosis of TENG.

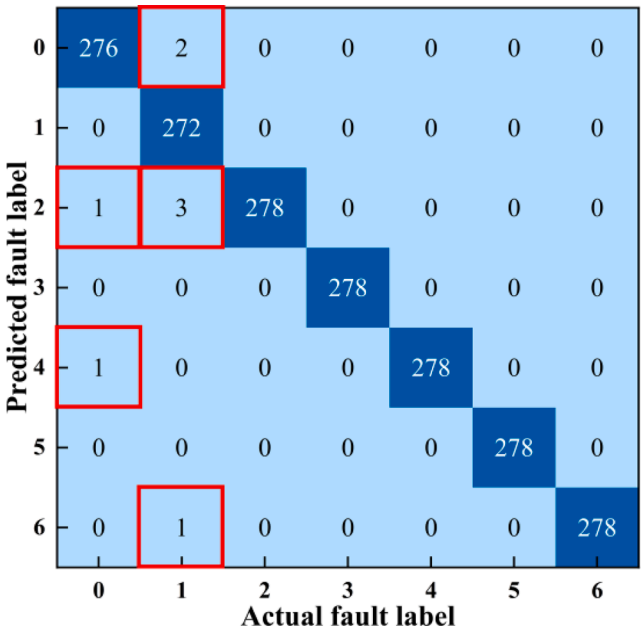

Fig. 15. Confusion matrix between the predicted and actual fault labels.

According to the training process of AttCNN, the reasons for AttCNN possesses promising fault diagnosis accuracy can be explained as follows. The training of AttCNN is data analysis for collected voltage signals, and then, the fault characteristics contained in the voltage signals can be extracted by AttCNN. Thereby the trained AttCNN can effectively perform online fault diagnosis for TENG with the real-time collected voltage signals. Based on the above analysis, it can be inferred that not only for TENG but also for other equipment with the collected signals containing feature information reflecting its status, AttCNN also possesses the potential to achieve good fault diagnosis performance. For instance, Fig. 16 shows a flow direction-velocity sensing device by applying TENG (Gong et al., 2019). The voltage of TENG and the velocity of flow have a one-to-one mapping relationship. If the flow velocity is outside the measured range, the voltage signal of TENG will be abnormal. According to the characteristic of AttCNN, once the AttCNN is trained with the voltage signal collected from the flow direction-velocity sensing device, the real-time status of this device can be identified by AttCNN with online voltage signals.

4.3. Comparison between AttCNN and classical fault diagnosis methods

4.3.1. Comparison between AttCNN and CNN

As described in Section 3.2, the difference between AttCNN and conventional CNN is the application of the attention mechanism in AttCNN, and AttCNN can effectively extract global correlation features in voltage signals with the attention mechanism. Aiming to evaluate the merit of the application of the attention mechanism in AttCNN, the fault diagnosis performance of AttCNN and conventional CNN is compared in this subsection. Notably, to present the role of the attention mechanism more intuitively, the CNN used for comparison is the AttCNN which is without the attention block.

On the basis of the training and validation sets described in Table 3, the training processes of AttCNN and CNN are depicted in Fig. 17. As shown in Fig. 17(a) and (b), although the training accuracy of CNN on the training and validation sets is finally convergence, the convergence efficiency of CNN is significantly worse than that of AttCNN. Moreover, the convergence results of the two methods are depicted in Fig. 18. It shows that the convergence performance of AttCNN is better than that of CNN in terms of the convergence value of accuracy and convergence epoch. Besides, as indicated in Fig. 17 and Fig. 18(b), although the training accuracy of CNN is convergence, the convergence stability of CNN is obviously worse than that of AttCNN. The reason can be explained as follows. Although local features in voltage signals can be extracted by CNN, the extracted feature is insufficient to reflect the status of TENG, resulting in that there exist obvious fluctuations in the training process of CNN.

With the trained AttCNN and CNN, the fault diagnosis results of the two methods on the testing set are depicted in Fig. 19, and the

Table 4
Fault diagnosis accuracy of different methods on the testing set.

Methods	Overall accuracy	*Label* 0	*Label* 1	*Label* 2	*Label* 3	*Label* 4	*Label* 5	*Label* 6
AttCNN	99.59%	99.28%	97.84%	100%	100%	100%	100%	100%
CNN	98.20%	98.56%	94.96%	97.84%	100%	100%	100%	96.04%

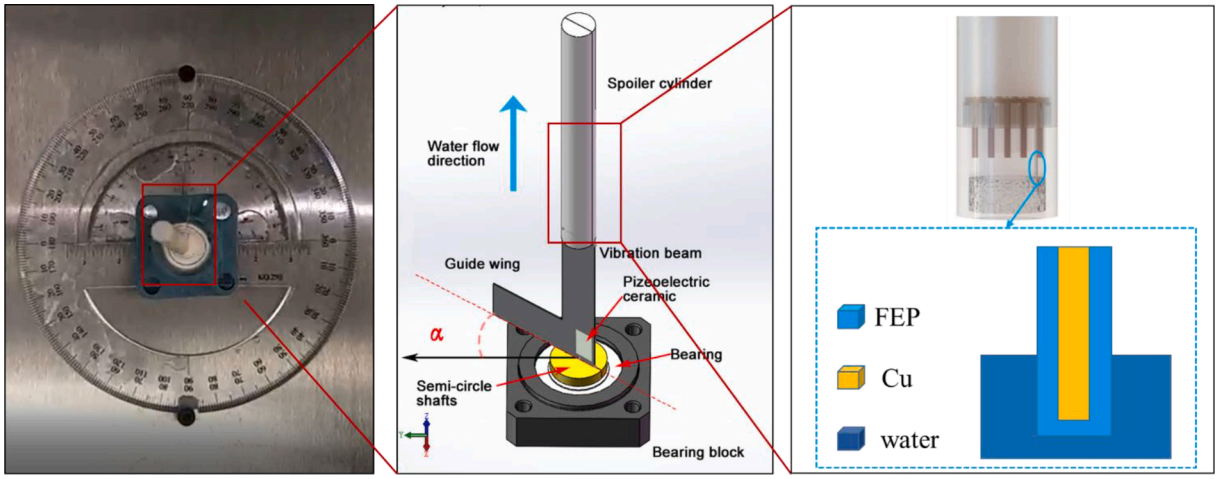

Fig. 16. A flow direction-velocity sensing device by applying TENG (Gong et al., 2019).

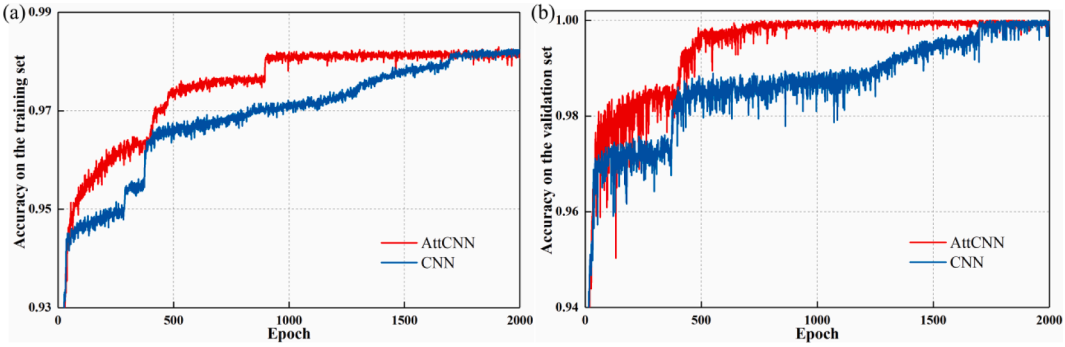

Fig. 17. Training processes of different methods: (a) the training accuracy on the training set; (b) the training accuracy on the validation set.

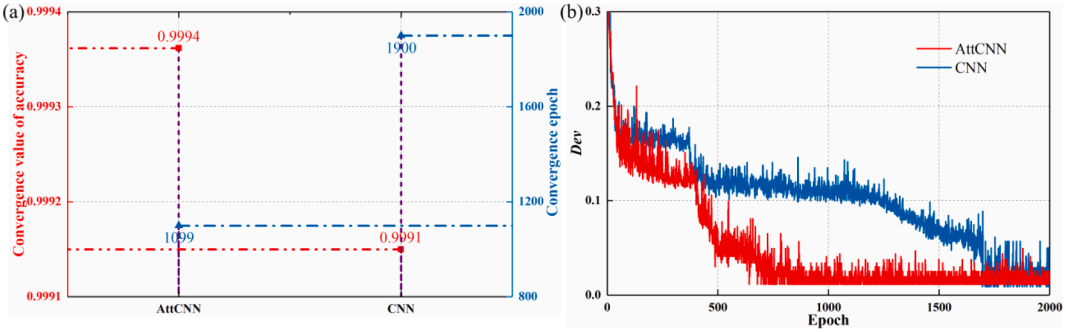

Fig. 18. The convergence results of different methods on the validation set: (a) the convergence results of the fault diagnosis accuracy; (b) the results of *Dev*.

corresponding fault diagnosis accuracy for each fault label is tabulated in Table 4. As shown in Fig. 19 and Table 4, there exist incorrect fault diagnoses for samples corresponding to four fault labels in the fault diagnosis results of CNN. Although the overall fault diagnosis accuracy of CNN reaches 98.20%, the fault diagnosis accuracies for the samples corresponding to fault *Label* 1 and *Label* 6 are 94.96% and 96.04%, respectively. Since the fault diagnosis accuracy of CNN for the case of fault *Label* 1 is less than 95%, CNN is unsuitable for performing the fault diagnosis of TENG.

According to the comparison results in Fig. 17, Fig. 18, and Fig. 19, the fault diagnosis performance of AttCNN is better than that of CNN. Hence, the results validate the superiority of the application of the attention mechanism in AttCNN, which reveals that the global correlation feature extracted by the attention mechanism is conducive to the

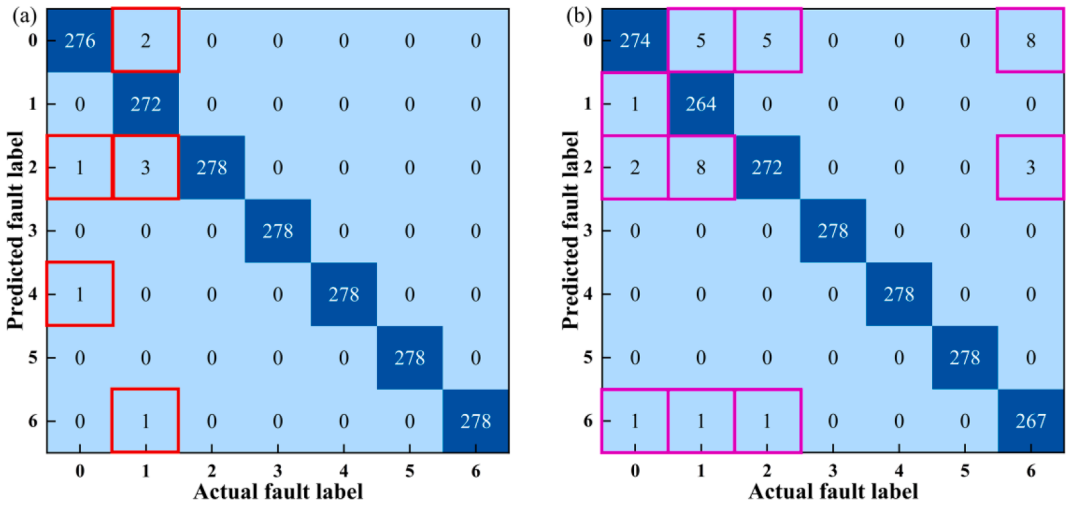

Fig. 19. Confusion matrix between the predicted and actual fault labels under different methods: (a) AttCNN; (b) CNN.

improvement of fault diagnosis performance for TENG.

4.3.2. Comparison between AttCNN and two classical fault diagnosis methods

Aiming to evaluate the superiority of AttCNN, the fault diagnosis performance between AttCNN and two machine learning methods is compared in this subsection.

As referred from Ref. (Jung, 2022), in the training and fault diagnosis processes of classical machine learning methods, the input and output of classical machine learning methods are feature vectors and labels, respectively. While the collected voltage signal of TENG is time sequences, the feature vector that characterizes the status of TENG needs to be extracted for the training of classical machine learning methods. Hence, aiming to compare the fault diagnosis performance of AttCNN and classical machine learning methods, an auto-encoder (AE) is used to adaptively extract feature vectors. With the training set tabulated in Table 3, the training process of AE is depicted in Fig. 20(a). Notably, in the training process of AE, the long short-term memory layer is used to convert signal sequences to feature vectors, and the number of neurons in each layer of AE is [50-12-3]. With the trained AE, the extracted 3D feature vectors are depicted in Fig. 20(b).

Based on the extracted feature vectors, the fault diagnosis performance of two classical machine learning methods is evaluated. Considering that support vector machine (SVM) and random forest (RF) are two commonly used machine learning methods for fault diagnosis (Arshad, Taqvi, Buang, & Awad, 2021; Xu et al., 2020), the fault diagnosis performance of SVM and RF is evaluated in this study.

With the extracted feature vectors and fault labels, SVM and RF are trained, respectively. Since the fault diagnosis performance of SVM and RF are also influenced by hyperparameters, the hyperparameter is also optimized in the training process of SVM and RF. Fig. 21 depicts the trends of the fault diagnosis accuracy of two methods on the training and testing sets under different cases of hyperparameters, where *gamma* and *max_depth* is the hyperparameter of SVM and RF, respectively. As depicted in Fig. 21, SVM with $gamma = 64$ and RF with $max\_depth = 34$ possess the best fault diagnosis performance on the testing set, and the fault diagnosis accuracy of SVM and RF is 79.92% and 89.91%, respectively.

As seen in Fig. 21, although the fault diagnosis accuracy of SVM and RF on the training set has the potential to be optimized to close to 1, the fault diagnosis accuracy of SVM and RF on the testing set is so worse that these two methods cannot be used in engineering practice. The reasons that the fault diagnosis accuracy of SVM and RF is worse than that of AttCNN can be explained as follows. The complex working principle of TENG results in that the feature vector characterizing the TENG status is complex, such as the feature vectors depicted in Fig. 20(b). Aiming to realize better fault diagnosis accuracy, the training of SVM and RF is prone to overfitting under the influence of complex feature vectors. And then, the generalization performance of SVM and RF is worse than that of AttCNN.

Based on the results in Table 4 and Fig. 21, AttCNN achieves a 24.61% and 10.77% performance enhancement for the overall fault diagnosis accuracy on the testing set compared to two classical machine learning methods SVM and RF, respectively. Hence, the superiority of

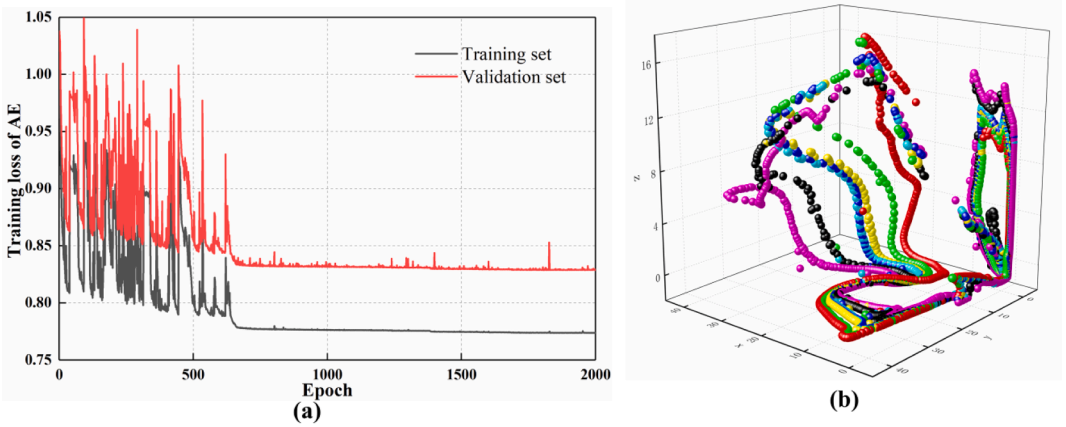

Fig. 20. The results of AE: (a) the training process of AE; (b) the feature vector extracted by AE.

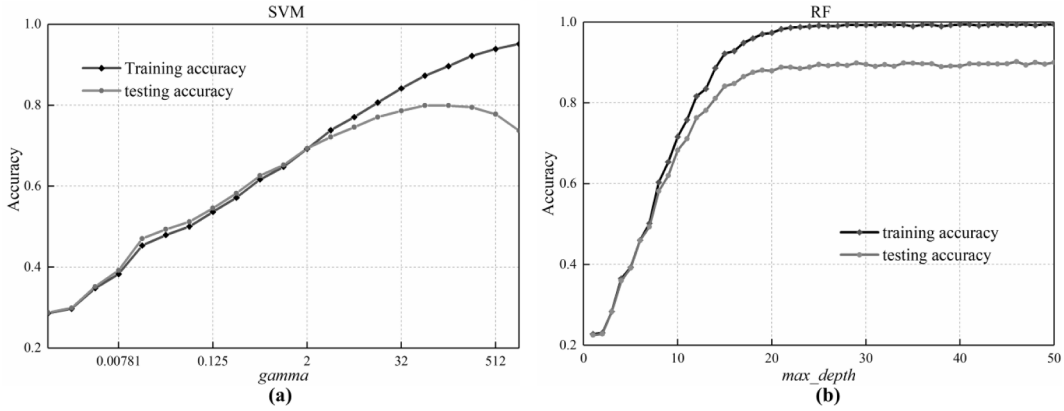

Fig. 21. Fault diagnosis accuracy on the training and testing sets: (a) the result of SVM under different values of *gamma*; (b) the result of RF under different values of *max_depth*.

AttCNN in terms of fault diagnosis accuracy and generalization performance is validated.

5. Conclusions

Considering the necessity of performing fault diagnosis for TENG, a novel deep learning framework based on AttCNN is proposed in this study. The global correlation features in voltage signals extracted by the attention mechanism in AttCNN can effectively reflect the status variation of TENG among different moments, and the feature information extracted by the convolutional network guarantees the fault diagnosis efficiency of TENG. Thereby the proposed method fills in the gaps in the field of fault diagnosis for TENG. The fault diagnosis performance of AttCNN for an experimental TENG is analyzed in the case study, and the main conclusions are drawn as follows:

(1) The hyperparameters *n_h* and *lr* have a certain impact on the fault diagnosis performance of AttCNN for TENG. It is suggested that field designers should pay more attention to the hyperparameter tuning in the design phase of AttCNN under different application scenarios.

(2) The fault diagnosis results indicate that AttCNN possesses a good performance in terms of the identification of the fault category and severity of TENG, thereby the application of AttCNN can provide more available information for the efficient maintenance of TENG. Moreover, the fault diagnosis results validate that AttCNN possesses a promising generalization performance for the fault diagnosis of TENG, illustrating the feasibility of the application of AttCNN for the fault diagnosis of TENG under different operating conditions. As the operating condition of TENG is usually uncertain, AttCNN is suitable to implement the real-time fault diagnosis of TENG.

(3) Compared with the conventional CNN, AttCNN achieves a 1.42% performance enhancement for the overall fault diagnosis accuracy on the testing set, more importantly, the fault diagnosis accuracy of AttCNN for each fault label exceeds 97.84%. The superiority of AttCNN benefits from the integration of the attention mechanism and convolutional networks. With the global correlation features in voltage signals extracted by the attention mechanism, AttCNN can effectively identify the status variation of TENG among any two moments.

(4) In this study, the fault diagnosis of TENG is realized by analyzing the voltage signals. As inferred from the principle of establishing the nonlinear relationship, other electric signals (current, transfer charge, etc.) that contain sufficient feature information characterizing the status of TENG are also available for providing data support for AttCNN. Moreover, AttCNN possesses the potential to implement fault diagnosis for various TENGs as long as the electric output signal can be collected.

Although the proposed deep learning framework contributes to the safe operation of TENG, there still exist limitations: AttCNN is a supervised learning algorithm, and the fault diagnosis performance of AttCNN for TENG may decline while sufficient electric output signals cannot be collected.

In future work, we will incorporate unsupervised learning algorithms with AttCNN to address these limitations.

CRediT authorship contribution statement

Hao Wu: Formal analysis, Writing – review & editing, Funding acquisition. **Xing'ang Xu:** Data curation, Methodology, Software, Writing – original draft, Writing – review & editing. **Chuanfu Xin:** Investigation, Formal analysis. **Yichen Liu:** Writing – original draft. **Runze Rao:** Visualization. **Zhongjie Li:** Conceptualization, Writing – review & editing, Supervision. **Dan Zhang:** Visualization. **Yongxi Wu:** Writing – original draft. **Senzhe Han:** Resources.

Declaration of Competing Interest

The authors declare that they have no known competing financial interests or personal relationships that could have appeared to influence the work reported in this paper.

Data availability

Data will be made available on request.

Acknowledgment

This work was supported by the Foundation of Kuaisu-Fuchi Program (Grant No. 80912020201), Qingnian Yingcai Qihang Program and National Natural Science Foundation of China (Grant No. 62001281).

References

Ajit, A., Acharya, K., & Samanta, A. (2020). A review of convolutional neural networks. *International Conference on Emerging Trends in Information Technology and Engineering, Ic-ETITE, 2020*, 1–5. https://doi.org/10.1109/ic-ETITE47903.2020.049

Ali, M., Din, Z., Solomin, E., Cheema, K. M., Milyani, A. H., & Che, Z. (2021). Open switch fault diagnosis of cascade H-bridge multi-level inverter in distributed power generators by machine learning algorithms. *Energy Reports, 7*, 8929–8942. https://doi.org/10.1016/j.egyr.2021.11.058

Arshad, U., Taqvi, S. A. A., Buang, A., & Awad, A. (2021). SVM, ANN, and PSF modelling approaches for prediction of iron dust minimum ignition temperature (MIT) based on the synergistic effect of dispersion pressure and concentration. *Process Safety and Environmental Protection, 152*, 375–390. https://doi.org/10.1016/j.psep.2021.06.001

Bello, I., Zoph, B., Le, Q., Vaswani, A., & Shlens, J. (2019). Attention augmented convolutional networks. *Proceedings of the IEEE International Conference on Computer Vision, 2019-Octob*, 3285–3294. https://doi.org/10.1109/ICCV.2019.00338.

Cheliotis, M., Gkerekos, C., Lazakis, I., & Theotokatos, G. (2019). A novel data condition and performance hybrid imputation method for energy efficient operations of marine systems. *Ocean Engineering, 188*(July), Article 106220. https://doi.org/10.1016/j.oceaneng.2019.106220

Chen, M., He, Y., & Sui, C. (2021). Open-switch fault diagnosis in three-level rectifiers based on selective calculation method for instant voltage deviation. *IET Power Electronics, 14*(5), 923–935. https://doi.org/10.1049/pel2.12075

Cheng, T., Gao, Q., & Wang, Z. L. (2019). The current development and future outlook of triboelectric nanogenerators: A survey of literature. *Advanced Materials Technologies, 4*(3), 1–7. https://doi.org/10.1002/admt.201800588

Chun, J., Ye, B. U., Lee, J. W., Choi, D., Kang, C. Y., Kim, S. W., … Baik, J. M. (2016). Boosted output performance of triboelectric nanogenerator via electric double layer effect. *Nature Communications, 7*(May), 1–9. https://doi.org/10.1038/ncomms12985

Fan, F. R., Tian, Z. Q., & Lin Wang, Z. (2012). Flexible triboelectric generator. *Nano Energy, 1*(2), 328–334. https://doi.org/10.1016/j.nanoen.2012.01.004

Feng, Y., Zheng, Y., Zhang, G., Wang, D., Zhou, F., & Liu, W. (2017). A new protocol toward high output TENG with polyimide as charge storage layer. *Nano Energy, 38* (June), 467–476. https://doi.org/10.1016/j.nanoen.2017.06.017

Gao, A., Feng, Z., & Liang, M. (2021). Permanent magnet synchronous generator stator current AM-FM model and joint signature analysis for planetary gearbox fault diagnosis. *Mechanical Systems and Signal Processing, 149*, Article 107331. https://doi.org/10.1016/j.ymssp.2020.107331

Gong, W., Chen, H., Zhang, Z., Zhang, M., & Gao, H. (2020). A data-driven-based fault diagnosis approach for electrical power DC-DC inverter by using modified convolutional neural network with global average pooling and 2-D feature image. *IEEE Access, 8*, 73677–73697. https://doi.org/10.1109/ACCESS.2020.2988323

Gong, Y., Shan, X., Luo, X., Pan, J., Xie, T., & Yang, Z. (2019). Direction-adaptive energy harvesting with a guide wing under flow-induced oscillations. *Energy, 187*, 115983. https://doi.org/10.1016/j.energy.2019.115983

Goodfellow, I., Bengio, Y., & Courville, A. (2016). *Deep learning*. MIT Press. https://www.deeplearningbook.org/.

Hidalgo-Leon, R., Urquizo, J., Silva, C. E., Silva-Leon, J., Wu, J., Singh, P., & Soriano, G. (2022). Powering nodes of wireless sensor networks with energy harvesters for intelligent buildings: A review. *Energy Reports, 8*, 3809–3826. https://doi.org/10.1016/j.egyr.2022.02.280

Hinton, G. E. (2012). A practical guide to training restricted boltzmann machines. *Neural Networks: Tricks of the Trade, LNTCS, 7700*, 599–619. https://doi.org/10.1007/978-3-642-35289-8_32

Huang, J., Fu, X., Liu, G., Xu, S., Li, X., Zhang, C., & Jiang, L. (2019). Micro/nano-structures-enhanced triboelectric nanogenerators by femtosecond laser direct writing. *Nano Energy, 62*(April), 638–644. https://doi.org/10.1016/j.nanoen.2019.05.081

Islam, M. R., Mekhilef, S., & Saidur, R. (2013). Progress and recent trends of wind energy technology. *Renewable and Sustainable Energy Reviews, 21*, 456–468. https://doi.org/10.1016/j.rser.2013.01.007

Jiao, J., Zhao, M., Lin, J., & Liang, K. (2020). A comprehensive review on convolutional neural network in machine fault diagnosis. *Neurocomputing, 417*, 36–63. https://doi.org/10.1016/j.neucom.2020.07.088

Jung, A. (2022). In *Machine Learning* (1st ed.). Singapore: Springer. https://doi.org/10.1007/978-981-16-8193-6.

Kim, M., Park, D., Alam, M. M., Lee, S., Park, P., & Nah, J. (2019). Remarkable output power density enhancement of triboelectric nanogenerators via polarized ferroelectric polymers and bulk MoS_2 composites. *ACS Nano, 13*(4), 4640–4646. https://doi.org/10.1021/acsnano.9b00750

LeCun, Y. A., Bottou, L., Orr, G. B., & Müller, K. R. (2012). Efficient backprop. In *Lecture Notes in Computer Science (including subseries Lecture Notes in Artificial Intelligence and Lecture Notes in Bioinformatics): Vol. 7700 LECTU* (Issue 1998). https://doi.org/10.1007/978-3-642-35289-8_3.

Lee, Y., Kim, W., Bhatia, D., Hwang, H. J., Lee, S., & Choi, D. (2017). Cam-based sustainable triboelectric nanogenerators with a resolution-free 3D-printed system. *Nano Energy, 38*(June), 326–334. https://doi.org/10.1016/j.nanoen.2017.06.015

Lei, Y., Yang, B., Jiang, X., Jia, F., Li, N., & Nandi, A. K. (2020). Applications of machine learning to machine fault diagnosis: A review and roadmap. *Mechanical Systems and Signal Processing, 138*, Article 106587. https://doi.org/10.1016/j.ymssp.2019.106587

Li, H., Pan, G., & Huang, Q. (2019). Transient analysis of the fluid flow on a pumpjet propulsor. *Ocean Engineering, 191*(September), Article 106520. https://doi.org/10.1016/j.oceaneng.2019.106520

Li, J., Li, B., Xu, J., Xiong, R., & Gao, W. (2018). Fully connected network-based intra prediction for image coding. *IEEE Transactions on Image Processing, 27*(7), 3236–3247. https://doi.org/10.1109/TIP.2018.2817044

Li, X., Cao, Y., Yu, X., Xu, Y., Yang, Y., Liu, S., … Wang, Z. L. (2022). Breeze-driven triboelectric nanogenerator for wind energy harvesting and application in smart agriculture. *Applied Energy, 306*(PA), Article 117977. https://doi.org/10.1016/j.apenergy.2021.117977

Liang, J., Zhang, K., Al-Durra, A., Muyeen, S. M., & Zhou, D. (2022). A state-of-the-art review on wind power converter fault diagnosis. *Energy Reports, 8*, 5341–5369. https://doi.org/10.1016/j.egyr.2022.03.178

Lin, M., Chen, Q., & Yan, S. (2014). Network in network. In *2nd International Conference on Learning Representations, ICLR 2014 - Conference Track Proceedings* (pp. 1–10). https://doi.org/10.48550/arXiv.1312.4400

Lin, Y., & Xu, X. (2023). Prediction of temperature distribution on piston crown surface of dual-fuel engines via a hybrid neural network. *Applied Thermal Engineering, 218* (August 2022), Article 119269. https://doi.org/10.1016/j.applthermaleng.2022.119269

Lin, Y., Xu, X., & Ye, C. (2021). Adaptive stochastic resonance quantified by a novel evaluation index for rotating machinery fault diagnosis. *Measurement: Journal of the International Measurement Confederation, 184*(February), Article 109920. https://doi.org/10.1016/j.measurement.2021.109920

Lone, S. A., Lim, K. C., Kaswan, K., Chatterjee, S., Fan, K. P., Choi, D., … Lin, Z. H. (2022). Recent advancements for improving the performance of triboelectric nanogenerator devices. *Nano Energy, 99*(February), Article 107318. https://doi.org/10.1016/j.nanoen.2022.107318

Qadir, Z., Khan, S. I., Khalaji, E., Munawar, H. S., Al-Turjman, F., Mahmud, M. A. P., … Le, K. (2021). Predicting the energy output of hybrid PV-wind renewable energy system using feature selection technique for smart grids. *Energy Reports, 7*, 8465–8475. https://doi.org/10.1016/j.egyr.2021.01.018

Qi, Y., Kuang, Y., Liu, Y., Liu, G., Zeng, J., Zhao, J., … Zhang, C. (2022). Kirigami-inspired triboelectric nanogenerator as ultra-wide-band vibrational energy harvester and self-powered acceleration sensor. *Applied Energy, 327*(October), Article 120092. https://doi.org/10.1016/j.apenergy.2022.120092

Qin, D., Huang, Q., Pan, G., Han, P., Luo, Y., & Dong, X. (2021). Numerical simulation of vortex instabilities in the wake of a preswirl pumpjet propulsor. *Physics of Fluids, 33* (5). https://doi.org/10.1063/5.0039935

Rumelhart, D. E., Hinton, G. E., & Williams, R. J. (1986). Learning representations by back-propagating errors. *Nature, 323*(6088), 533–536. https://doi.org/10.1038/323533a0

Vaswani, A., Shazeer, N., Parmar, N., Uszkoreit, J., Jones, L., Gomez, A. N., Kaiser, Ł., & Polosukhin, I. (2017). Attention is all you need. *Advances in Neural Information Processing Systems*, *2017-Decem*(Nips), 5999–6009.

Wang, J., Jiang, Z., Sun, W., Xu, X., Han, Q., & Chu, F. (2022). Yoyo-ball inspired triboelectric nanogenerators for harvesting biomechanical energy. *Applied Energy, 308*(December 2021), Article 118322. https://doi.org/10.1016/j.apenergy.2021.118322

Wang, X., Gao, Q., Zhu, M., Wang, J., Zhu, J., Zhao, H., … Cheng, T. (2022). Bioinspired butterfly wings triboelectric nanogenerator with drag amplification for multidirectional underwater-wave energy harvesting. *Applied Energy, 323*(June), Article 119648. https://doi.org/10.1016/j.apenergy.2022.119648

Wiesler, S., & Ney, H. (2011). A convergence analysis of log-linear training. *Advances in Neural Information Processing Systems 24: 25th Annual Conference on Neural Information Processing Systems 2011, NIPS 2011*, 1–9.

Xiang, H., Yang, J., Cao, X., & Wang, N. (2022). Flexible and highly sensitive triboelectric nanogenerator with magnetic nanocomposites for cultural heritage conservation and human motion monitoring. *Nano Energy, 101*(June), Article 107570. https://doi.org/10.1016/j.nanoen.2022.107570

Xin, C., Li, Z., Zhang, Q., Peng, Y., Guo, H., & Xie, S. (2022). Investigating the output performance of triboelectric nanogenerators with single/double-sided interlayer. *Nano Energy, 100*(June), Article 107448. https://doi.org/10.1016/j.nanoen.2022.107448

Xu, S., Tao, S., He, Y., & Chai, Y. (2022). Multiple open-circuit fault diagnosis for back-to-back converter of PMSG wind generation system based on instantaneous amplitude estimation. *Diangong Jishu Xuebao/Transactions of China Electrotechnical Society, 37* (2), 433–444. https://doi.org/10.19595/j.cnki.1000-6753.tces.200775.

Xu, X., Zhao, Z., Xu, X., Yang, J., Chang, L., Yan, X., & Wang, G. (2020). Machine learning-based wear fault diagnosis for marine diesel engine by fusing multiple data-driven models. *Knowledge-Based Systems, 190*, Article 105324. https://doi.org/10.1016/j.knosys.2019.105324

Xu, Z., Li, D., Wang, K., Liu, Y., Wang, J., Qiu, Z., … Li, F. (2022). Stomatopod-inspired integrate-and-fire triboelectric nanogenerator for harvesting mechanical energy with ultralow vibration speed. *Applied Energy, 312*(August 2021), Article 118739. https://doi.org/10.1016/j.apenergy.2022.118739

Xue, Z. Y., Li, M. S., Xiahou, K. S., Ji, T. Y., & Wu, Q. H. (2019). A data-driven diagnosis method of open-circuit switch faults for PMSG-based wind generation system. *Proceedings of the 2019 IEEE 12th International Symposium on Diagnostics for Electrical Machines, Power Electronics and Drives, SDEMPED 2019*, 481–487. https://doi.org/10.1109/DEMPED.2019.8864922.

Xue, Z. Y., Xiahou, K. S., Li, M. S., Ji, T. Y., & Wu, Q. H. (2020). Diagnosis of multiple open-circuit switch faults based on long short-term memory network for DFIG-based wind turbine systems. *IEEE Journal of Emerging and Selected Topics in Power Electronics, 8*(3), 2600–2610. https://doi.org/10.1109/JESTPE.2019.2908981

Yang, L., & Shami, A. (2020). On hyperparameter optimization of machine learning algorithms: Theory and practice. *Neurocomputing, 415*, 295–316. https://doi.org/10.1016/j.neucom.2020.07.061

Yang, Z., Chai, Y., Yin, H., & Tao, S. (2018). LPV model based sensor fault diagnosis and isolation for permanent magnet synchronous generator in wind energy conversion systems. *Applied Sciences (Switzerland), 8*(10). https://doi.org/10.3390/app8101816

Yuan, M., Yu, W., Jiang, Y., Ding, Z., Zhang, Z., Zhang, X., & Xie, Y. (2022). Triboelectric nanogenerator metamaterials for joint structural vibration mitigation and self-powered structure monitoring. *Nano Energy, 103*(PA), Article 107773. https://doi.org/10.2139/ssrn.4165508

Zhang, Q., Xin, C., Shen, F., Gong, Y., Zi, Y. L., Guo, H., … Wang, Z. L. (2022). Human body IoT systems based on the triboelectrification effect: Energy harvesting, sensing, interfacing and communication. *Energy and Environmental Science, 3688–3721*. https://doi.org/10.1039/d2ee01590k

Zhao, C., Liu, D., Wang, Y., Hu, Z., Zhang, Q., Zhang, Z., … Xu, M. (2022). Highly-stretchable rope-like triboelectric nanogenerator for self-powered monitoring in marine structures. *Nano Energy, 94*(December 2021), Article 106926. https://doi.org/10.1016/j.nanoen.2022.106926

Zhao, Y., Fan, Z., Bi, C., Wang, H., Mi, J., & Xu, M. (2022). On hydrodynamic and electrical characteristics of a self-powered triboelectric nanogenerator based buoy under water ripples. *Applied Energy, 308*(December 2021), Article 118323. https://doi.org/10.1016/j.apenergy.2021.118323

Zhu, J., Ji, S., Yu, J., Shao, H., Wen, H., Zhang, H., … Lee, C. (2022). Machine learning-augmented wearable triboelectric human-machine interface in motion identification

and virtual reality. *Nano Energy, 103*(PA), Article 107766. https://doi.org/10.1016/j.nanoen.2022.107766

Zhu, J., Sun, Z., Xu, J., Walczak, R. D., Dziuban, J. A., & Lee, C. (2021). Volatile organic compounds sensing based on Bennet doubler-inspired triboelectric nanogenerator and machine learning-assisted ion mobility analysis. *Science Bulletin, 66*(12), 1176–1185. https://doi.org/10.1016/j.scib.2021.03.021

Zhu, J., Wen, H., Zhang, H., Huang, P., Liu, L., & Hu, H. (2023). Recent advances in biodegradable electronics- from fundament to the next-generation multi-functional, medical and environmental device. *Sustainable Materials and Technologies, 35*(August 2022), e00530. https://doi.org/10.1016/j.susmat.2022.e00530

Zhu, J., Yang, Y., Zhang, H., Zhao, Z., Hu, T., & Liu, L. (2023). More than energy harvesting in electret electronics- moving toward next-generation functional system. *Advanced Functional Materials*, 2214859. https://doi.org/10.1002/adfm.202214859

Zhu, J., Zhu, M., Shi, Q., Wen, F., Liu, L., Dong, B., … Lee, C. (2020). Progress in TENG technology—A journey from energy harvesting to nanoenergy and nanosystem. *EcoMat, 2*(4), 1–45. https://doi.org/10.1002/eom2.12058